EVALUATION OF NEW FERRITIC STEELS BY SYNCHROTRON RADIATION

Michael Santella
Oak Ridge National Laboratory, 1 Bethel Valley Road, Oak Ridge, TN 37931-6096
Email: santellaml@ornl.gov; Telephone: 865-574-4805

John Shingledecker
Oak Ridge National Laboratory, 1 Bethel Valley Road, Oak Ridge, TN 37931-6155
Email: shingledecjp@ornl.gov; Telephone: 865-574-4929

Robert Swindeman
Oak Ridge National Laboratory, 1 Bethel Valley Road, Oak Ridge, TN 37931-6155
Email: swindemanrw@ornl.gov; Telephone: 865-574-5108

BACKGROUND

During creep testing, weldment specimens generally rupture in the fine grained heat affected zone regions of microstructure at times considerably shorter than those of either the base metal or the weld metal. This behavior in the Cr-Mo steels is commonly referred to as Type IV cracking. The heat-affected zone creep behavior effectively limits the lifetimes of welded components made from these steels. Recent studies[1] at the Steel Research Center of the National Institute for Materials Science (NIMS) in Japan indicate that Type IV cracking can be eliminated by alloying 9Cr steels with relatively high concentrations of B, and low concentrations of N. The reasons for this unusual and potentially significant behavior are unclear, but they appear related to the nucleation and growth of austenite during heating and cooling cycles in weld heat-affected zones. One possibility is that the B addition suppresses austenite nucleation and growth during heat-affected zone thermal cycles. A second possible mechanism is that the base metal contains retained austenite which is distributed so that the original coarse austenite grain size is regenerated during heat-affected zone thermal cycles. To date, however, efforts to identify retained austenite in the base metal microstructure have been inconclusive.

This report describes experiments done in collaboration with researchers at NIMS to use unique Department of Energy facilities and Oak Ridge National Laboratory expertise to examine the austenite transformation behavior of Type-IV-cracking resistant 9Cr steels being developed in Japan.

EXPERIMENTAL DETAILS

The chemical compositions of the two 9Cr steels that were used for the synchrotron diffraction experiment are given in Table 1. The alloys were prepared at NIMS and supplied in normalized and tempered conditions: 1 h @ 1080°C + 1 h @ 800°C for the boron-steel N130B, and 2 h @ 1070°C + 2 h @ 780°C for the P92 steel. The specimens of the steels were 1 mm x 4.8 mm x 112 mm with the diffracting surfaces metallographically polished.

Table 1. Chemical compositions

	Element (wt%)										
ID	C	Si	Mn	Cr	W	Mo	Co	Nb	V	N	B
N130B	0.077	0.30	0.49	8.97	2.87	---	2.91	0.046	0.18	0.0015	0.013
P92	0.09	0.16	0.47	8.72	1.87	0.45	---	0.06	0.21	0.050	0.002

The specimens were held in copper grips so that they functioned as resistors in an electrical circuit. A thermocouple was spot welded to the backside of each specimen at the location where diffraction occurred. The thermocouple measured temperature (± 0.2°C) and provided feedback to a controller that permitted programming of temperature histories. The base of one side of the specimen holder was mounted on bearings and it was spring-loaded. This arrangement produced a slight tension force to permit the specimen to freely expand as it was heated. In its current configuration, the heating stage is mounted in a vacuum chamber that minimizes oxidation. For the 9Cr steels, there was no visible sign of oxidation after heating. After each of the thermal cycles the specimens were just as shiny as when they were unpackaged.

The incident x-rays were provided by the UNICAT X-33 undulator beamline at the Advanced Photon Source (Argonne National Laboratory, Argonne, Illinois). The radiation was filtered with a 0.25-mm Ti foil (1.7% transmission) to avoid saturating the detectors, and it was monochromatized by Si (111) crystals to a wavelength λ = 0.041328 nm. At this energy, x-rays penetrate about 0.16 mm into steel, so diffraction from the near-surface region is relatively weak. The x-rays were incident at a 5° glancing angle resulting in a footprint on the sample of about 1 x 0.25 mm. This arrangement of equipment permitted a 2D image of the diffracted x-rays to be recorded by a charge-coupled device (CCD) as shown schematically in Fig. 1. The CCD detector was positioned 330 mm behind the specimen outside of the vacuum chamber. X-ray data were captured by the detector by integrating the diffracted beams over a 1 s exposure. Another 2 s were required to clear the data from the CCD detector and transfer it to a computer. Thus, it was possible to capture a complete diffraction pattern approximately every 3 s.

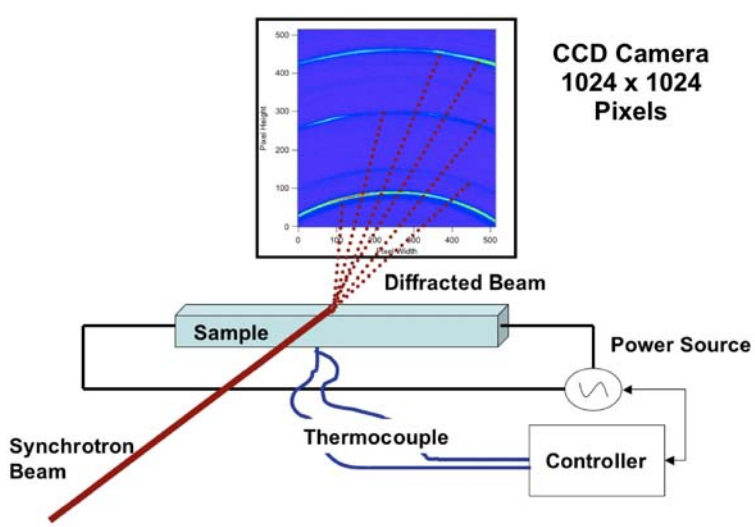

Fig. 1. Schematic illustration of process of capturing a diffraction pattern on the CCD camera.

TEMPERATURE HISTORY DETAILS

This first experiment was conducted by attempting to heat specimens of the N130B and P92 steels through simulated heat-affected zone thermal cycles. The thermal cycles were calculated using a 3D Rosenthal analysis for 25-mm-thick steel plate and the welding parameters of 2000 W (200 A x 10 V), translation speed of 1.6 mm/s, and 100°C preheat. The calculations were done to determine the variation of peak temperature with distance from the weld centerline. To select peak temperatures for the diffraction experiments, the calculated peak temperatures were then compared to the A_1 and A_3 temperatures estimated from equilibrium thermodynamics calculations. The calculated A_1 and A_3 temperatures are given in Table 2. These transformation temperatures are also indicated on Fig. 2 which shows the variation of calculated HAZ peak temperatures with distance from the weld centerline.

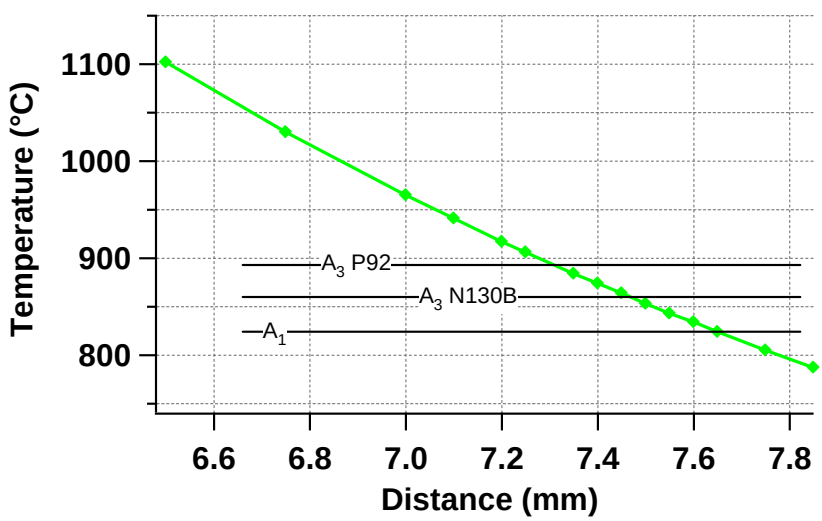

Fig. 2. Variation of calculated peak temperatures in the heat-affected zone with distance from weld centerline. The A_1 and A_3 transformation temperatures for N130B and P92 steel are also shown.

Table 2. A_1 and A_3 transformation temperatures estimated from equilibrium thermodynamics calculations

	Temperature (°C)	
Steel	A_1	A_3
N130B	825	860
P92	826	893

Based on these considerations 4 peak temperatures were selected for programming into the temperature controller: (1) 843°C, just above the A_1 of both steels, (2) 874°C, above A_3 of N130B and high in the ferrite + austenite phase field of P92, (3) 917°C, above the A_3 of both steels, and (4) 1100°C, high in the austenite phase field of both steels. Because of the limitation of data collection at 3 s intervals the initial heating rates were reduced and a 3 s dwell was programmed at the peak temperature. The heating rates were adjusted to reach the peak temperatures in 9 s in order to capture diffraction patterns during heating. The 3 s dwell was added to capture at least one diffraction pattern at the peak temperatures.

Ultimately, the temperature controller did not follow the programmed history as closely as desired. In particular, the programmed peak temperatures were exceeded. Differences between programmed and actual peak temperature during the diffraction experiments are shown in Table 3.

Table 3. Comparison of programmed and actual peak temperatures

Experiment	Peak temperature (°C) Programmed	Actual
N130Bexp01	843	923
N130Bexp02	874	944
N130Bexp03	917	991
N130Bexp04	1100	1122
P92exp01	843	896
P92exp02	874	927
P92exp03	917	975
P92exp04	1100	1088

RESULTS

The data from each experiment are presented in two formats. In one case, image representations of the data were constructed to show how diffracted intensity varied with both time and d-spacings. In a second case, the data are shown as the variations of diffracted intensities with d-spacings. Image representations of the data for the N130Bexp01 specimen are shown in Fig. 3.

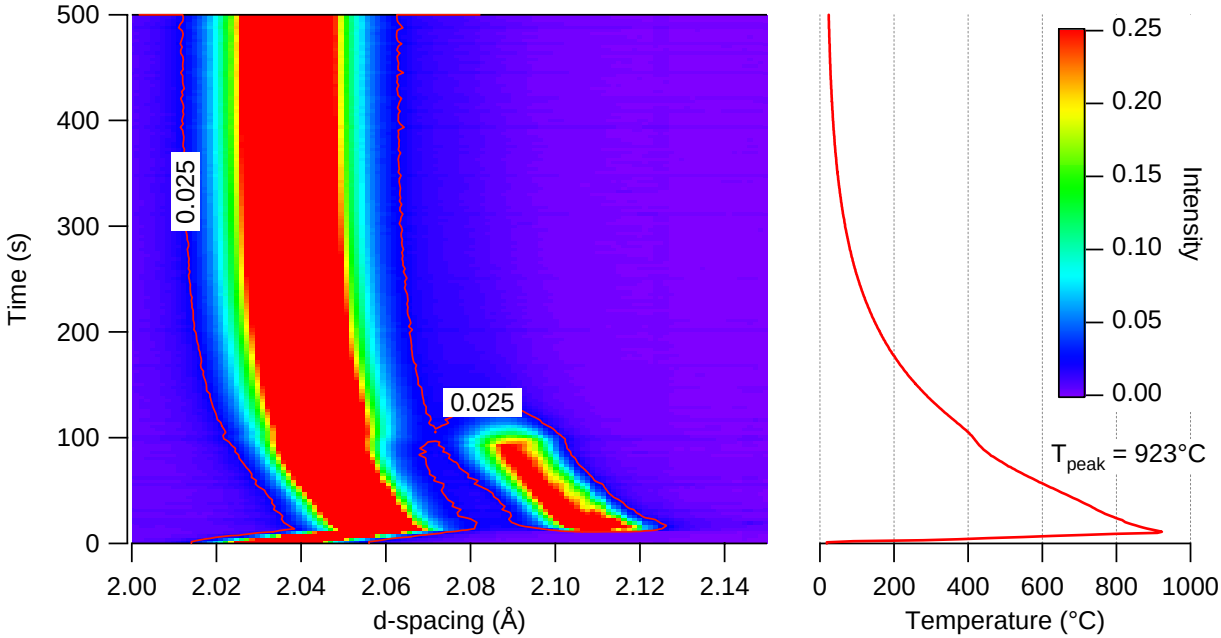

Fig. 3. Image representation of the diffraction data from N130B steel captured at 3 s intervals during heating to and cooling from a peak temperature of 923°C. High intensity diffraction is indicated by red and background intensity by blue. The intensity at the lower d-spacing is from ferrite; that at the higher d-spacing from austenite.

In Fig. 3 the intensity scale was weighted to emphasize lower values. Also, the image includes a contour for intensity threshold, in this case a very low value of 0.025. The d-spacing scale also was limited to highlight a region where both {110} ferrite and {111} austenite reflections are present in close proximity. The data show that no austenite was detected before or during heating. Diffracted intensity from austenite only appeared after the specimen temperature reached its peak value of 923°C. Even though this temperature exceeded the A_3, ferrite never completely disappeared from the microstructure. The image representations also suggest that austenite completely disappeared during cooling of this specimen.

The sequence of diffraction pattern segments shown in Fig. 4 highlight the behavior illustrated by Fig. 3. Diffraction from the starting normalized and tempered N130B steel is shown in Fig. 4 (a). No austenite was detected by diffraction in the starting material. Figure 4 (b) confirms that ferrite never completely dissolved during this temperature history and actually was present at a greater amount than was austenite at 923°C. Figure 4 (c) shows that austenite was present to relatively low temperatures, ~ 400°C, during cooling as expected. Figure 4 (d) is for material cooled to about 30°C at the end of the thermal cycle. Comparison of Figs. 4 (a) & (d) indicates that if austenite was present in the microstructure after this temperature history, then its amount was similar to that which originally existed in the microstructure before heating.

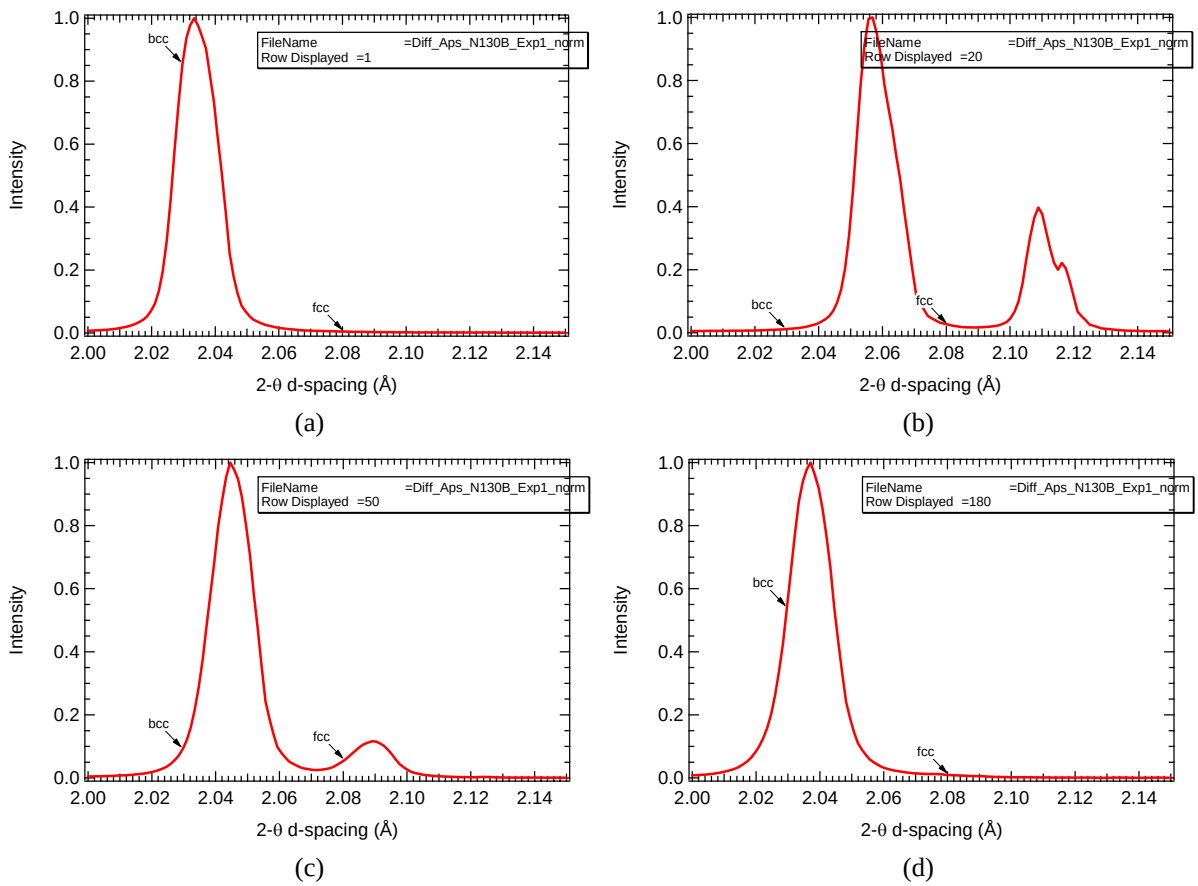

Fig. 4. Variations of diffracted intensity from {110} ferrite and {111} austenite reflections for specimen N130Bexp01 at temperature conditions of (a) before heating, (b) just beyond the peak temperature of 923°C, (c) near 400°C on cooling, and, (d) near room temperature after cooling.

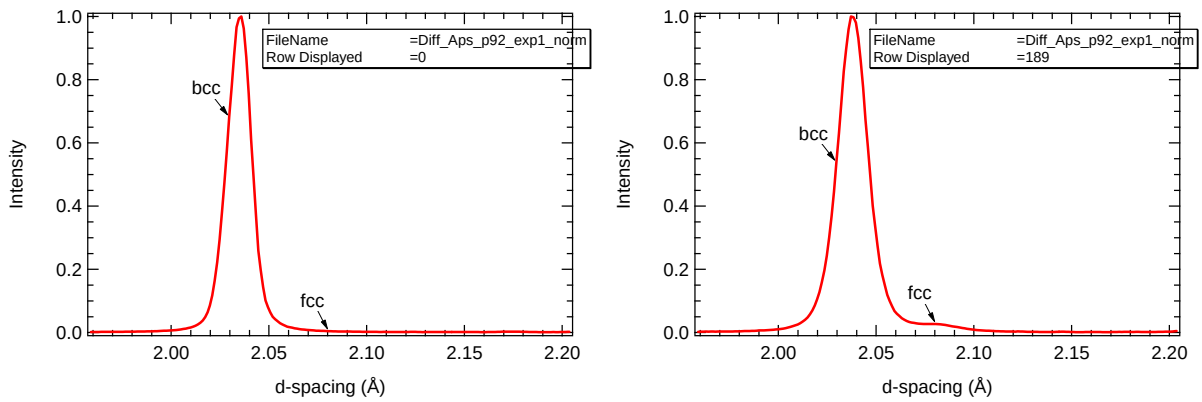

(a) (b)

Fig. 5. Variations of diffracted intensity from {110} ferrite and {111} austenite reflections for specimen P92exp01 at temperature conditions of (a) before heating, (b) near room temperature after cooling.

Similar observations of the P92 behavior are highlighted in Fig. 5. Diffraction from the starting quenched and tempered P92 steel is shown in Fig. 5 (a). No austenite was detected in the starting condition. The condition of this alloy after heating to and cooling from a peak temperature of 896°C is shown in Fig. 5 (b). After this treatment there is a small level of diffracted intensity at the expected position of {111} austenite reflection. Unlike the N130B steel, it appears that this HAZ thermal history resulted in retained austenite.

A summary of observations from the diffraction experiments is given in Table 4. The diffraction data show that both steels were heated with the simulated HAZ temperature histories to well above their equilibrium A_3 temperatures before the transformation of ferrite (α) to austenite (γ) was complete. They also indicate that P92 has a greater tendency to retain austenite after the heating/cooling cycles.

Table 4. Summary of synchrotron diffraction results for N130B and P92 steels

Experiment	Actual T_{peak} (°C)	$\alpha \rightarrow \gamma$ completed	Retained γ
N130Bexp01	923	No	No
N130Bexp02	944	No	No
N130Bexp03	991	Yes	Yes
N130Bexp04	1122	Yes	Yes
P92exp01	896	No	Yes
P92exp02	927	No	Yes
P92exp03	975	Yes	Yes
P92exp04	1088	Yes	Yes

DISCUSSION

The equilibrium amounts of precipitate phases predicted for the N130B and P92 steels are shown in Fig. 6. The predictions indicate that above about 900°C the N130B steel contains only a small amount of M(C,N) phase that has a composition near NbC. In contrast, the composition of the M(C,N) in P92 is

near NbN at high temperatures and near VN at low temperatures. Additionally, M(C,N) is present in a much greater amount in the P92 than it is in the N130B. Below about 800°C, P92 contains about 0.3 wt% of M(C,N) compared to about 0.05 wt% in N130B. The predicted solution temperature of M(C,N) in P92 is also higher, 1280°C compared to about 1150°C in N130B. Since M(C,N) is used to control austenite grain size in many carbon steels, it is possible that it could be a factor in inhibiting austenite grain growth in P92. The M_3B_2 phase may also complicate the behavior of the N130B steel. The thermodynamics indicate that it will be stable at a relatively high fraction of about 0.2 wt%, but only in the range of 840-1120°C. Only very small amounts of boride phases, below about 0.03 wt% total, are present in the P92.

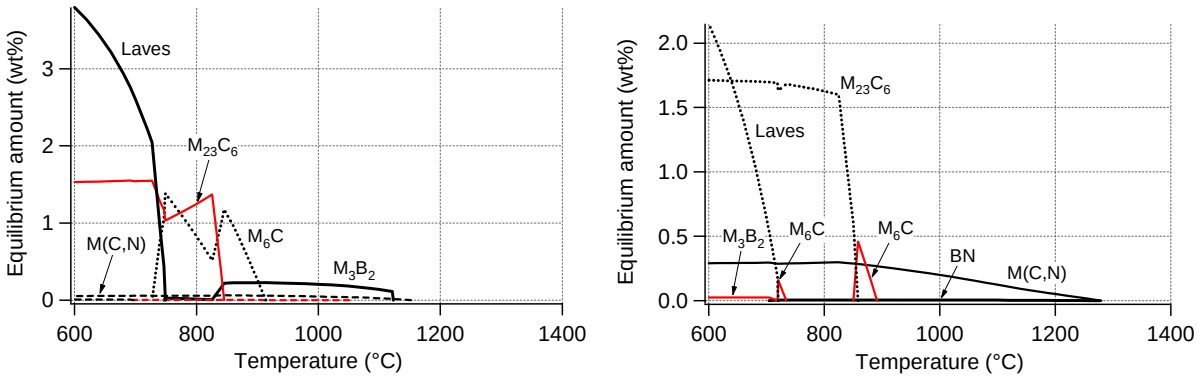

(a) (b)

Fig. 6. Variations with temperature of the predicted equilibrium amounts of precipitate phases for (a) N130B and (b) P92

An alternate interpretation of the diffraction data is that austenite nucleation was inhibited in N130B compared to P92. Estimates of the fractions of ferrite and austenite based on the areas of diffraction peaks are shown in Fig. 7 for N130Bexp01 with peak temperature of 923°C, and in Fig. 8 for P92exp01 with peak temperature of 896°C. Constraints on the peak fitting procedures limited the phase fraction estimates to the cooling portions of temperature histories. The maximum amount of austenite formed in N130B was estimated at near 30%; that in P92 was near 80%. This occurred even though the amount by which A_3 was exceeded was greater for N130B than it was for P92. The lower austenite amounts in N130B are consistent with austenite nucleation being more sluggish in this alloy. Similar behavior was also found when comparing N130Bexp02 with P92exp02. The specimens that were heated to higher peak temperatures all transformed completely to austenite so similar comparisons were not possible.

SUMMARY

Specimens of P92 and a Type-IV-resistant 9Cr steel were examined using synchrotron diffraction. Initial results indicate that the resistance to Type IV cracking may be related to austenite transformation behavior as material is heated during welding. These experiments were conducted as part of a collaboration with the National Institute for Materials Science (NIMS) in Japan.

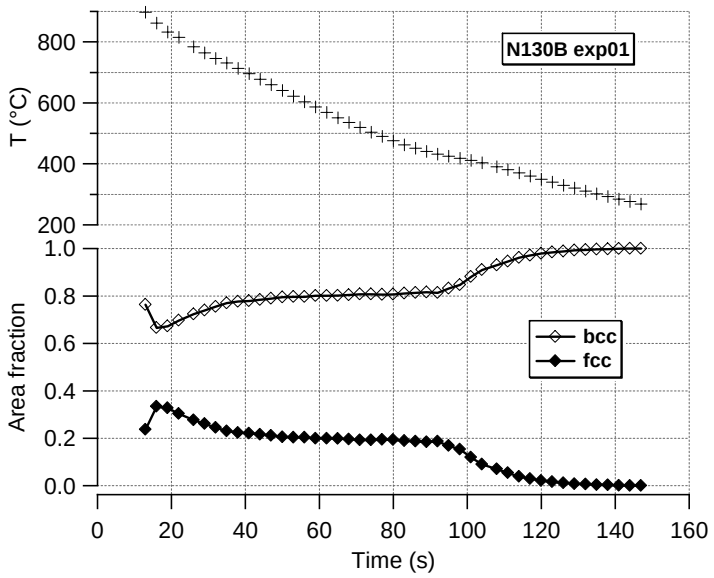

Fig. 7. Variations of temperature and peak area fractions, i.e., amounts of bcc ferrite and fcc austenite, estimated from diffracted intensities for specimen N130Bexp01

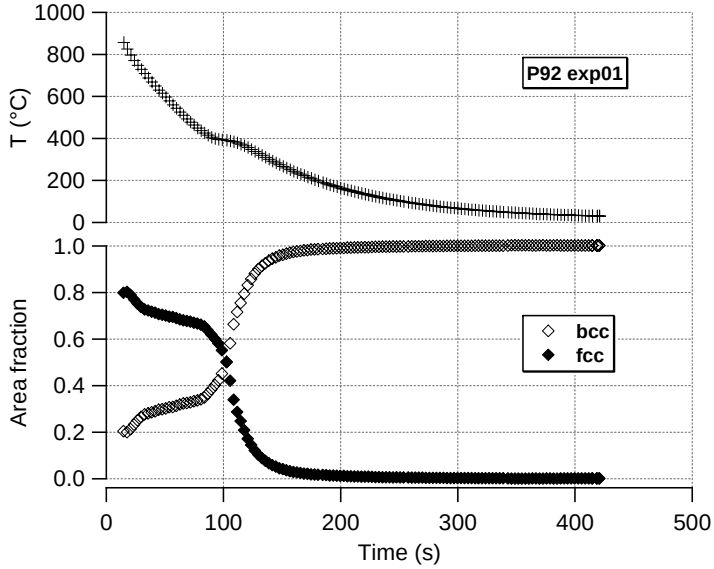

Fig. 8. Variations of temperature and peak area fractions, i.e., amounts of bcc ferrite and fcc austenite, estimated from diffracted intensities for specimen P92Bexp01

REFERENCES

1. M. Kondo, M. Tabuchi, S. Tsukamoto, F. Yin, and F. Abe, "Suppression of Type IV Failure in High-B Low-N 9Cr-3W-3Co-NbV Steel Welded Joint," in *Fourth International Conference on Advances in Materials Technology for Fossil Power Plants*, EPRI, 2004.